Quantum Interference in Wilkinson Power Dividers

Osmery Hernández, Angel Ortega-Gomez, Mikel Bravo, and Iñigo Liberal*

Scaling up quantum technologies entails the challenge of developing large-scale and high-performance photonic quantum networks. Engineering novel optical components, with a compact footprint and advanced functionalities, might help addressing this challenge by reducing the size and complexity of optical networks. Here, quantum interference phenomena in Wilkinson power dividers (WPDs), a popular element of microwave networks, is investigated. It is theoretically demonstrated that WPDs grant access to coherent perfect absorption (CPA) quantum state transformations (single photon CPA, coherent absorption of N00N states, two-photon nonlinear absorption, and absorption of coherence in squeezed light) in CPA networks with a smaller footprint and a reduced number of elements. Additionally, it is shown how a WPD can be designed in a pure silicon-on-insulator platform by taking advantage of radiative losses. These findings might represent an important step forward in the development of CPA quantum networks.

1. Introduction

The development of photonic quantum technologies is leading to optical networks of increasing size and complexity.[1] Examples of this current trend are state-of-the-art photonic systems for multidimensional entanglement generation,[2] quantum information processing,[3] quantum computing,[4] and simulation.[5] However, the realization of large-scale photonic networks poses significant challenges, which might hinder scaling up quantum technologies toward practical applications. For this reason, there is a motivation to rethink optical networks, searching for new ideas that might simplify the implementation of quantum technologies. For example, the use of new components with advanced functionalities in optical networks might lead to simplified architechtures with a reduced footprint and/or a smaller number of elements.

Harnessing absorption has proved to provide optical networks with new features. In particular, coherent perfect absorption (CPA), that can be loosely defined as phase-dependent perfect absorption[6,7] leverages interference phenomena, using absorption as a resource, to enable a number of photonic applications such as all-optical data processing[8,9] and sensing,[10] as well as dynamic control over photocurrent[11] and photothermal[12] excitations. Additionally, CPA allows for generalized quantum state engineering,[13] where the set of available transformations is not restricted to unitary processes. Examples of absorption-assisted quantum state transformations include the anticoalescence of photons and anti-Hong–Ou–Mandel effect,[13–16] allowing for the exchange between bosonic and fermionic statistics, single-photon CPA,[13,17] coherent control of absorption of N00N states,[18,19] probabilistic two-photon absorption or nonlinear absorption,[20] and quantum absorption of coherence in squeezed states.[21]

Several material and technological platforms have been proposed to investigate CPA, including plasmonic[22,23] and all-dielectric[24,25] metasurfaces, surface plasmon polariton devices,[14,18,26] integrated photonic circuits containing plasmonic elements,[27–29] phase-change materials,[7,30–32] and photonic doping of epsilon-near-zero (ENZ) media.[33,34] Quantum CPA experiments[13–19] have been mostly focused around the concept of lossy beamsplitters[20,35] implemented with different plasmonic nanosctructures.

Following the motivations of using advanced devices to simplify network architectures and harnessing the benefits of CPA, in this work, we investigate quantum interference phenomena taking place within a Wilkinson power divider (WPD).[36] WPDs are popular elements in microwave engineering applications, known for providing power combining/splitting capabilities, while ensuring impedance matching and isolation between their input ports.[36] The main contribution of our work consists of demonstrating that, using a WPD, CPA quantum state transformations can be implemented with a single and compact device, with a unique output channel and no backward reflections, allowing for reducing the footprint and number of elements (additional photon counters, beamsplitters, circulators) of CPA quantum networks. In addition, we provide the design of a WPD in a pure silicon-on-insulator (SOI) platform, that is, a silicon-based design without the need of plasmonic materials. We believe that our results represent an important step forward in the implementation of CPA quantum networks. In addition, we believe that our findings are a great example on how the complexity of quantum optical networks can be reduced with the use of advanced devices.

O. Hernández, A. Ortega-Gomez, M. Bravo, I. Liberal
Department of Electrical, Electronic and Communications Engineering
Institute of Smart Cities (ISC)
Public University of Navarre (UPNA)
Pamplona 31006, Spain
E-mail: inigo.liberal@unavarra.es

The ORCID identification number(s) for the author(s) of this article can be found under https://doi.org/10.1002/lpor.202200095

**ADVANCED
SCIENCE NEWS**

www.advancedsciencenews.com
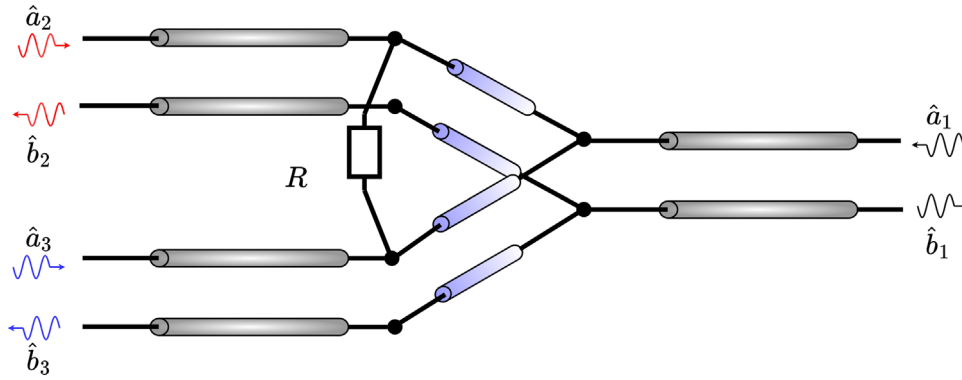
www.lpr-journal.org

LASER
& PHOTONICS
REVIEWS

Figure 1. Schematic representation/circuit diagram of a WPD.

2. Classical Mode of Operation of a Wilkinson Power Divider

We start by revisiting the classical mode of operation of a Wilkinson power divider (WPD), specifically in its equal splitting version. The schematic representation/circuit diagram of the device is depicted in **Figure 1**, and its classical scattering matrix can be written as[36]

$$S = \frac{1}{\sqrt{2}} \begin{bmatrix} 0 & 1 & 1 \\ 1 & 0 & 0 \\ 1 & 0 & 0 \end{bmatrix} \quad (1)$$

We can readily check from the scattering matrix (1) that the WPD is a reciprocal ($S_{ij} = S_{ji}, \forall i, j$) and lossy ($SS^\dagger \neq I$) three-port device, which has all its ports matched ($S_{ii} = 0, \forall i$). Additionally, the device provides isolation between ports 2 and 3 ($S_{23} = S_{32} = 0$). Moreover, the classical mode of operation of a WPD can be best appreciated by performing a singular value decomposition (SVD) of its scattering matrix,[37–39] leading to the factorization

$$S = U\Sigma_S V^\dagger \quad (2)$$

with

$$U = \frac{1}{\sqrt{2}} \begin{bmatrix} \sqrt{2} & 0 & 0 \\ 0 & 1 & -1 \\ 0 & 1 & 1 \end{bmatrix} \quad \Sigma_S = \begin{bmatrix} 1 & 0 & 0 \\ 0 & 1 & 0 \\ 0 & 0 & 0 \end{bmatrix}$$

$$V = \frac{1}{\sqrt{2}} \begin{bmatrix} 0 & \sqrt{2} & 0 \\ 1 & 0 & -1 \\ 1 & 0 & 1 \end{bmatrix} \quad (3)$$

Note that U and V are unitary matrices (i.e., $UU^\dagger = I$, $VV^\dagger = I$), and therefore their columns (and rows) conform an orthonormal basis of $\mathbb{C}^N$. From this perspective, the SVD can be visualized as a one-to-one mapping between vectors of two different orthonormal basis of $\mathbb{C}^N$, that is, $V \to U$. This mapping is scaled by a real and positive factor that corresponds to the diagonal entries of Σ_S. Therefore, by comparing each column of U with their corresponding column in V, the SVD decomposition provides an intuitive visualization of the classical response of a device.

For the particular case of a WPD, the SVD identifies three modes of operation: i) The mapping between the first columns of V and U shows that the symmetrical excitation of the second and third ports leads to the combination of all the power into the first port, that is, the device can operate as a lossless power combiner. ii) The mapping between the second columns of V and U shows that the excitation from the first port results in an equal division of the input power into ports 2 and 3, that is, the device can operate as a lossless power divider. iii) The mapping between the third columns of V and U shows that the out-of-phase excitation of ports 2 and 3 leads to the total absorption of the input power. Since such perfect absorption critically depends on the phase difference between the signals at ports 2 and 3, it can be concluded that the device also operates as a coherent perfect absorber (CPA).

3. Quantum Input–Output Relations for a Wilkinson Power Divider

Having revisited the classical mode of operation of a Wilkinson power divider from the perspective of the SVD, we next move to address quantum interference phenomena in such device. To this end, we must first identify the quantum input–ouput relations.[40–43] For a lossless device, the quantum input–output relations are defined by the classical scattering matrix, $\hat{b} = S\hat{a}$, where $\hat{a} = [\hat{a}_1, \dots, \hat{a}_N]^T$ and $\hat{b} = [\hat{b}_1, \dots, \hat{b}_N]^T$ are column vectors that contain bosonic operators describing the input and output photonic modes, respectively. However, for a lossy device, the input–ouput relations need to be generalized in order to keep track of the excitations absorbed by the device[40–43]

$$\begin{bmatrix} \hat{b} \\ \hat{g} \end{bmatrix} = \Lambda \begin{bmatrix} \hat{a} \\ \hat{f} \end{bmatrix} \quad (4)$$

where $\hat{f} = [\hat{f}_1, \dots, \hat{f}_N]^T$ and $\hat{g} = [\hat{g}_1, \dots, \hat{g}_N]^T$ are column vectors that contain bosonic operators describing the input and output excitations within the device. These operators obey bosonic commutation relations, $[\hat{f}_m, \hat{f}_n^\dagger] = [\hat{g}_m, \hat{g}_n^\dagger] = \delta_{mn}$, $[\hat{f}_m, \hat{f}_n] = [\hat{g}_m, \hat{g}_n] = 0$, and effectively represent the internal excitations within the device.[40,41] Λ is an extended scattering matrix characterizing the quantum input–output relations for a lossy device. The extended scattering matrix Λ can be compactly written as follows[42]

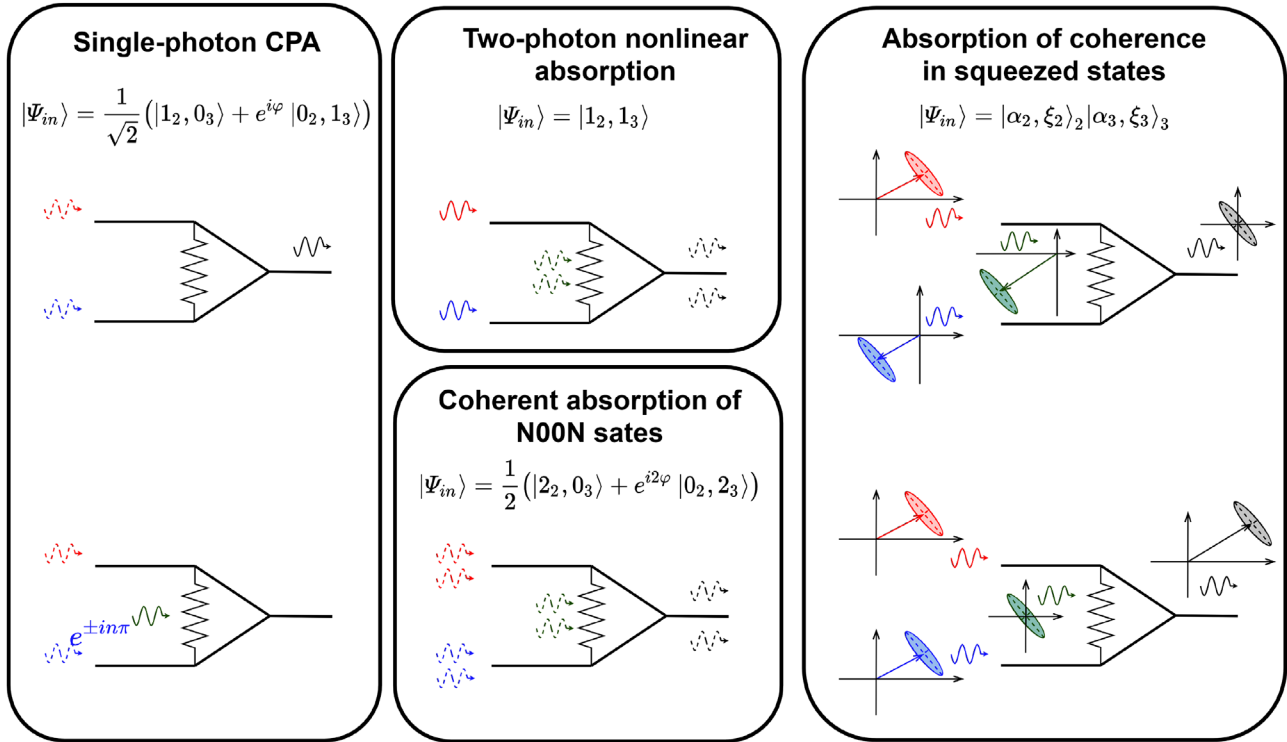$$\Lambda = \begin{bmatrix} S & A \\ -A & S \end{bmatrix} \quad (5)$$

Figure 2. Sketch of interference-assisted absorption phenomena in a WPD excited with nonclassical light states. Representations include phenomena of interest in the few-photon and multiple-photon regimes.

where the "absorption" matrix A has been factorized by the same unitary matrices that the scattering matrix, $A = U\Sigma_A V^\dagger$, but with singular values given by $\Sigma_A = (I - \Sigma_S)^{1/2}$. For the scattering matrix of a Wilkinson power divider, given by Equation (1), the "absorption" matrix is specifically given by

$$A = \frac{1}{2}\begin{bmatrix} 0 & 0 & 0 \\ 0 & 1 & -1 \\ 0 & -1 & 1 \end{bmatrix} \qquad (6)$$

Next, the extended scattering matrix Λ of the device is obtained by introducing Equation (6) into Equation (5). From Equation (5) and considering the unitary property of Λ, we can obtain the inverse replacement rules for the creation operators in a WPD

$$\hat{a}_1^\dagger \rightarrow \frac{1}{\sqrt{2}}\left(\hat{b}_2^\dagger + \hat{b}_3^\dagger\right) \qquad (7)$$

$$\hat{a}_2^\dagger \rightarrow \frac{1}{\sqrt{2}}\hat{b}_1^\dagger - \frac{1}{\sqrt{2}}\hat{g}_-^\dagger \qquad (8)$$

$$\hat{a}_3^\dagger \rightarrow \frac{1}{\sqrt{2}}\hat{b}_1^\dagger + \frac{1}{\sqrt{2}}\hat{g}_-^\dagger \qquad (9)$$

where we have defined the superposition operator $\hat{g}_-^\dagger = (\hat{g}_2^\dagger - \hat{g}_3^\dagger)/\sqrt{2}$. As we will exemplify in the next section, the knowledge of these inverse input–output relations enables the analysis of arbitrary quantum interference effects. In particular, one

starts with an input state defined by a function of creation operators of the input optical modes: $|\psi_{in}\rangle = F_{in}(\hat{a}_1^\dagger, \hat{a}_2^\dagger, \hat{a}_3^\dagger)|0\rangle$, and, then, the output state is found by replacing the creation operators by using the inverse input–output relations (7)–(9), $|\psi_{out}\rangle = F_{out}(\hat{b}_1^\dagger, \hat{b}_2^\dagger, \hat{b}_3^\dagger, \hat{g}_1^\dagger, \hat{g}_2^\dagger, \hat{g}_3^\dagger)|0\rangle$.

4. Quantum Interference in a Wilkinson Power Divider

Once the quantum input–ouput relations of a WPD have been established, it is possible to evaluate different quantum interference phenomena taking place in a WPD. Due to the interest of CPA for quantum state engineering,[13–23] we will focus on configurations in which ports 2 and 3 act as input ports, while port 1 is the output port. As we will show, a WPD is capable of reproducing quantum state transformations based on CPA in a single and compact device, as well as using a single output port. Therefore, it can implement all CPA quantum state transformations with a smaller footprint on the quantum network, as well as with a reduced number of components. **Figure 2** schematically depicts and summarizes our findings, which are the basic quantum interference processes taking place in a WPD, which we address in detail in the following subsections.

4.1. Single-Photon CPA

Let us start by analyzing the excitation of a WPD with a single-photon superposition state impinging on ports 2 and 3 with a

2200095 (3 of 10)

phaseshift φ between the arms. In other words, the input state is given by

$$|\Psi_{in}\rangle = \frac{1}{\sqrt{2}} \left(\hat{a}_2^\dagger + e^{i\varphi} \hat{a}_3^\dagger \right) |0\rangle \tag{10}$$

Next, the output state is determined by applying the inverse input–output relations (7)–(9) into the input state (10), leading to

$$|\Psi_{out}\rangle = \frac{1}{2} \hat{b}_1^\dagger \left(1 + e^{i\varphi} \right) - \frac{1}{2} \hat{g}_-^\dagger \left(1 - e^{i\varphi} \right) |0\rangle \tag{11}$$

It is clear from Equation (11) that the output state can be manipulated by changing the relative phase φ between the arms. Varying the relative phase φ allows for a coherent control of the output state, which results in output states ranging from perfect transparency to perfect absorption. Specifically, given no phase difference between input beams, that is, $\varphi = 0$, occurs a perfect transmission of the input photon through output port 1, that is, $|\Psi_{out}\rangle = \hat{b}_1^\dagger |0\rangle$. Furthermore, the input photon will always be absorbed, that is, $|\Psi_{out}\rangle = -\hat{g}_-^\dagger |0\rangle$, for a phase difference $\varphi = \pm n\pi$, leading to the coherent perfect absorption of the input state.

Single-photon CPA has been experimentally demonstrated by using a lossy beamsplitter as the absorption element.[22,23] In addition, the setups are complemented either by using circulators[22] or lossless beamsplitters forming an stationary wave,[23] as well as two photon counters. A WPD poses several technological advantages. First, a WPD enables the same functionality with a reduced footprint. All interference and photon routing processes take place in a compact device, and there is no need for additional elements such as circulators and/or lossless beamsplitters. Moreover, the isolation properties of the WPD ensure that there is no reflection back into ports 2 and 3, so that there are no detrimental effects associated with unwanted photons recirculating into the network. Finally, since the output photons are routed to the same output port, only one detector would be needed to perform the experiment. Therefore, implementing single-photon CPA in a WPD is a good example of how advanced devices enable the simplification of quantum networks.

4.2. Two-Photon Nonlinear Absorption

Another intriguing effect that we can access in a WPD arises from the simultaneous excitation of the ports 2 and 3 of the device with single-photon states, that is

$$|\Psi_{in}\rangle = \hat{a}_2^\dagger \hat{a}_3^\dagger |0\rangle \tag{12}$$

The corresponding output state

$$|\Psi_{out}\rangle = \frac{1}{2} \left(\hat{b}_1^{\dagger 2} - \hat{g}_-^{\dagger 2} \right) |0\rangle \tag{13}$$

reveals the occurrence of a nonlinear absorption event, where both photons either bunch together through output port 1, or both are absorbed within the device. As it can be noted from the output state, both events occur with equal probability. In other words, a probabilistic absorption of the two photons takes place. The process is nonlinear in the sense that if one of the photons

is absorbed, so will the other. Therefore, there is no possibility that exactly one photon survives, as their associated probability amplitudes interfere destructively. Nonlinear two-photon absorption was first theoretically predicted for a lossy beamsplitter.[20] To the best of our knowledge, it has not been experimentally demonstrated yet. However, experimental studies on related photon statistics of two-photon interference in setups containing a lossy beamsplitter have been carried out.[14,15] Again, the use of a WPD would simplify the device, facilitating the experimental demonstration of two-photon nonlinear absorption.

4.3. Coherent Absorption of N00N States

A related coherent absorption effect takes place when a WPD is excited by a N00N state, that is, a superposition state of N photons impinging on either port 2 or port 3, with a phaseshift φ between the arms. In particular, the input state for a two-photon $N = 2$ N00N state can be written as follows

$$|\Psi_{in}\rangle = \frac{1}{2} \left(\hat{a}_2^{\dagger 2} + e^{i2\varphi} \hat{a}_3^{\dagger 2} \right) |0\rangle \tag{14}$$

It is clear from Equation (14) that the phaseshift between the arms φ is enlarged to $N\varphi$ on the N00N state, a feature that can be exploited for sensing with enhanced resolution.[44] By using the inverse relations (8)–(9), we find that the output state can be written as follows

$$|\Psi_{out}\rangle = \frac{1}{4} \left[\hat{b}_1^{\dagger 2} \left(1 + e^{i2\varphi} \right) + \hat{g}_-^{\dagger 2} \left(1 + e^{i2\varphi} \right) - 2\hat{b}_1^\dagger \hat{g}_-^\dagger \left(1 - e^{i2\varphi} \right) \right] |0\rangle \tag{15}$$

The output state in Equation (15) describes a superposition state where we might get three different outcomes: i) both photons being transmitted, ii) both photons being absorbed, or iii) one-photon survival and one-photon absorption. Additionally, the phase shift φ provides a degree of freedom in the engineering of the probability amplitudes of each outcome in Equation (15). In this way, a relative phase $\varphi = 0$ leads to the output state: $|\Psi_{out}\rangle = \frac{1}{2}(\hat{b}_1^{\dagger 2} + \hat{g}_-^{\dagger 2})|0\rangle$, that is, probabilistic two-photon nonlinear absorption, as discussed in the previous section. On the other hand, a relative phase $\varphi = \pm(2n+1)\frac{\pi}{2}$ leads to the deterministic absorption of exactly one photon, that is, $|\Psi_{out}\rangle = -\hat{b}_1^\dagger \hat{g}_-^\dagger |0\rangle$. Regimes of total transmission or total absorption of the input photons are forbidden for a N00N state. Therefore, by changing the phase between the input arms it is possible to switch between probabilistic two-photon nonlinear absorption to deterministic single photon absorption. Similar effects have been theoretically predicted[35] and experimentally demonstrated[17,18] for setups based on lossy beamsplitters. Again, we find that quantum coherent absorption functionalities can be implemented with a simplified network.

4.4. Quantum Absorption/Manipulation of Coherence in Squeezed States

It is also worthwhile to assess the interaction of nonclassical light states with a WPD beyond the few-photon regime. An example of
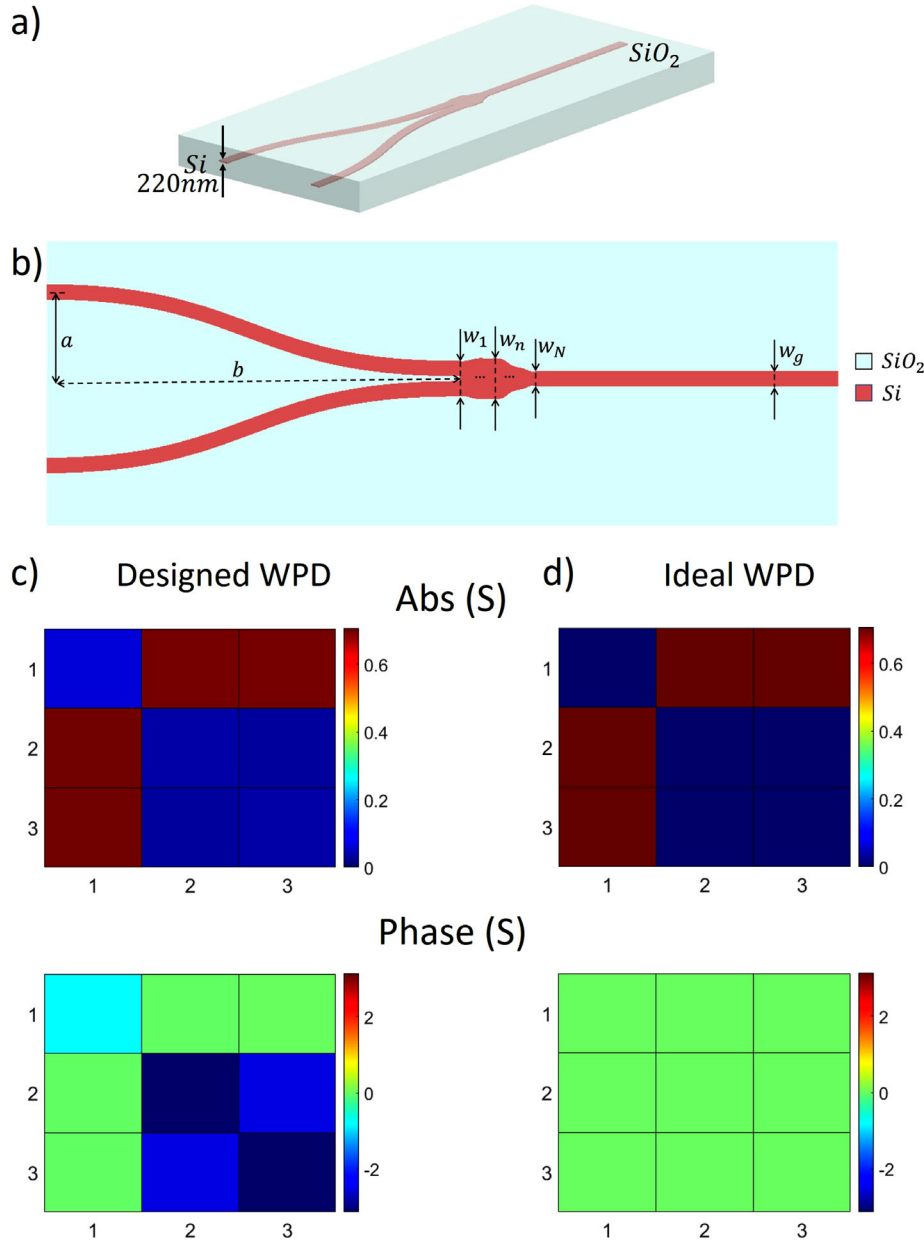
Figure 3. a) FDTD Lumerical 3D model of the designed WPD. b) Additional details of the geometry. c,d) Representation of the absolute value (top panel) and phase (bottom panel) of the scattering matrix of c) the designed WPD, and d) the ideal WPD. A global phase factor of $\exp(-i1.4532)$ has been applied to the scattering matrix of the designed WPD.

particular relevance for quantum sensing and quantum metrology is that of squeezed coherent states, which enable the reduction of statistical noise on one quadrature component at the expense of increasing it on the conjugate quadrature.[44,45]

We start by studying the case of single-mode squeezed coherent states in both inputs arms of the WPD, so that the input state is given by

$$|\Psi_{in}\rangle = \hat{S}_2(\xi_2)\,\hat{D}_2(\alpha_2)\,\hat{S}_3(\xi_3)\,\hat{D}_3(\alpha_3)\,|0\rangle \qquad (16)$$

where we have defined the displacement operator $\hat{D}_n(\alpha_n) = \exp(\alpha_n\hat{a}_n^\dagger - \alpha_n^*\hat{a}_n)$ corresponding to the coherent part, the quan-

tum description of a classical field with complex magnitude α_n, with an average number of photons $|\alpha_n|^2$.[46] We have also introduced the squeezing operator $\hat{S}_n(\xi_n) = \exp\frac{1}{2}(\xi_n^*\hat{a}_n^2 - \xi_n\hat{a}_n^{\dagger 2})$ with squeezing parameter ξ_n.

Since the input photonic operators commute, we can group together the displacement and squeezing operators in Equation (16) and apply the inverse input–output relations. In this manner, the squeezed and coherent parts of the input state can be separately controlled. On the one hand, the coherent part follows the behavior of classical waves. On the other hand, the squeezed part reduces to a nontrivial combination of single- and two-mode squeezed states. However, for the particular case of input states

with equal squeezing parameters $\xi_2 = \xi_3 = \xi$, we can rearrange the results into displacement and squeezing operators for output photonic and device modes to obtain the following output state

$$|\Psi_{\text{out}}\rangle = \hat{S}_1(\xi)\,\hat{D}_1\left(\frac{\alpha_2 + \alpha_3}{\sqrt{2}}\right)\hat{S}_-(\xi)\,\hat{D}_-\left(\frac{\alpha_3 - \alpha_2}{\sqrt{2}}\right)|0\rangle \qquad (17)$$

From Equation (17), we can conclude that the output state consists of a single-mode squeezed coherent state in both the output photonic and absorption channels. Moreover, the squeezing parameter of both the output photonic and absorption channels remains the same as that in the input states. By contrast, the coherent parts scale differently. In particular, the output photonic part scales as $(\alpha_2 + \alpha_3)/\sqrt{2}$ while the absorption part scales as $(\alpha_3 - \alpha_2)/\sqrt{2}$. Therefore, a lossless power combiner is obtained for in-phase signals $\alpha_2 = \alpha_3$ (see Figure 2, right top panel), while out-of-phase signals $\alpha_2 = -\alpha_3$ lead to coherent perfect absorption (see Figure 2, right bottom panel). We can then identify two extreme cases on the excitation of the WPD with squeezed states. The excitation with states where the squeezing parameters are equal but the coherent factors are in phase opposition, that is, $\xi_2 = \xi_3 = \xi$ and $\alpha_2 = -\alpha_3 = \alpha$, leads to absorption of the coherent part of the incident beams, and the output photonic state is a squeezed vacuum state: $|\Psi_{\text{out}}\rangle = \hat{S}_1(\xi)\hat{S}_-(\xi)\hat{D}_-(-\sqrt{2}\alpha)|0\rangle$. On the other hand, the symmetrical excitation of the device, that is, $\xi_2 = \xi_3 = \xi$ and $\alpha_2 = \alpha_3 = \alpha$, leads to a squeezed coherent state with strengthened coherent part: $|\Psi_{\text{out}}\rangle = \hat{S}_1(\xi)\hat{D}_1(\sqrt{2}\alpha)\hat{S}_-(\xi)|0\rangle$. In this manner, it is possible to deterministically control the coherent part of a squeezed coherent state, while maintaining its squeezing properties.

Quantum absorption of coherence in squeezed states was previously theoretically studied in the context of lossy beamsplitters,[21] though to the best of our knowledge it has not been experimentally demonstrated yet. Our results demonstrate that the same functionality can be obtained with a device with a reduced footprint, isolation ensuring that no photons are reflected backward, and a single output channel, which might facilitate the experimental verification of this effect.

In addition, the WPD suggests a further extension on the theory of quantum control of coherence of squeezed states. Specifically, the topology of a WPD is particularly well suited for its excitation with a two-mode squeezed state, in which either the amplitude difference or the phase-sum quadratures are squeezed.[45,47] The input state of the system for a two-mode squeezed coherent state is given by

$$|\Psi_{\text{in}}\rangle = \hat{S}_{2,3}(\xi)\,\hat{D}_2(\alpha_2)\,\hat{D}_3(\alpha_3)|0\rangle \qquad (18)$$

where $\hat{S}_{2,3} = \exp(\xi^*\hat{a}_2\hat{a}_3 - \xi\hat{a}_2^\dagger\hat{a}_3^\dagger)$ is the two-mode squeezing operator. The associated output state can be written as follows:

$$|\Psi_{\text{out}}\rangle = \hat{S}_1(\xi)\,\hat{D}_1\left(\frac{\alpha_2 + \alpha_3}{\sqrt{2}}\right)\hat{S}_-(-\xi)\,\hat{D}_-\left(\frac{\alpha_3 - \alpha_2}{\sqrt{2}}\right)|0\rangle \qquad (19)$$

It can be concluded from Equation (19) that the output photonic state is a single-mode squeezed coherent state with squeezing parameter ξ, and controlled coherent part $(\alpha_2 + \alpha_3)/\sqrt{2}$. In

Table 1. Design parameters of the WPD.

Parameter	Value [μm]	Parameter	Value [μm]
a	4.1	w_6	1.6
b	16.23	w_7	1.6
w_g	0.6	w_8	1.46
w_1	1.4	w_9	1.1
w_2	1.4	w_{10}	0.9
w_3	1.51	w_{11}	0.8
w_4	1.6	w_{12}	0.6
w_5	1.6	w_{13}	0.6

this manner, a WPD empowers two simultaneous operations: i) transforming a two-mode squeezed state into a single-mode squeezed state, and ii) at the same time deterministically controlling its coherent part. Moreover, the WPD guarantees that there will be no backreflection independently of the choice of the parameters of the coherent and incoherent parts of the state, α_2, α_3, ξ. Again, we find that the WPD enables the implementation of multiple operations in a reduced footprint, while providing a network topology protected against backreflections.

5. Integrated Photonics Wilkinson Power Divider

Wilkinson power dividers (WPD) are a popular element for classical microwave engineering applications.[36] However, its application for quantum technologies is far less explored. Due to the similarities in the technology, the implementation of a WPD in quantum optical systems based on superconducting circuits should be straightforward. However, the implementation of a WPD at optical frequencies requires from additional development. In this section, we provide with the design of a silicon photonics WPD, demonstrating that the quantum state transformations proposed above can be implemented in standard integrated photonic circuits.

As schematically depicted in Figure 1a, a WPD basically consists of the junction of two tranmission lines, also interconnected with a shunt resistor. From this perspective, it appears that the most direct route toward implementing an integrated photonics WPD would be to start with one of the many Y-branches developed in silicon photonics, and to add a metallic nanoparticle or a 2D material, effectively acting as a resistance. Unfortunately, the use of exotic materials adds additional nanofabrications steps, and it might prevent the fabrication by large-scale semiconductor nanofacturers. Scaling up the complex optical networks in which photonic quantum technologies are based requires from the use of more standard silicon platforms. In the following, we show that a WPD in a pure silicon-on-insulator (SOI) platform can be developed by harnessing radiative losses.

Essentially, SOI Y-branches consist of the junction of waveguides, where the geometry of the intersection is designed to improve the performance in terms of insertion loss, bandwidth and footprint.[48–50] Following ref. [48], we numerically designed a tapered geometry so that the device effectively acts as a WPD when operating with the first higher-order TM eigenmode. As shown in **Figure 3**a, the device consists of a Y-branch splitter imple-
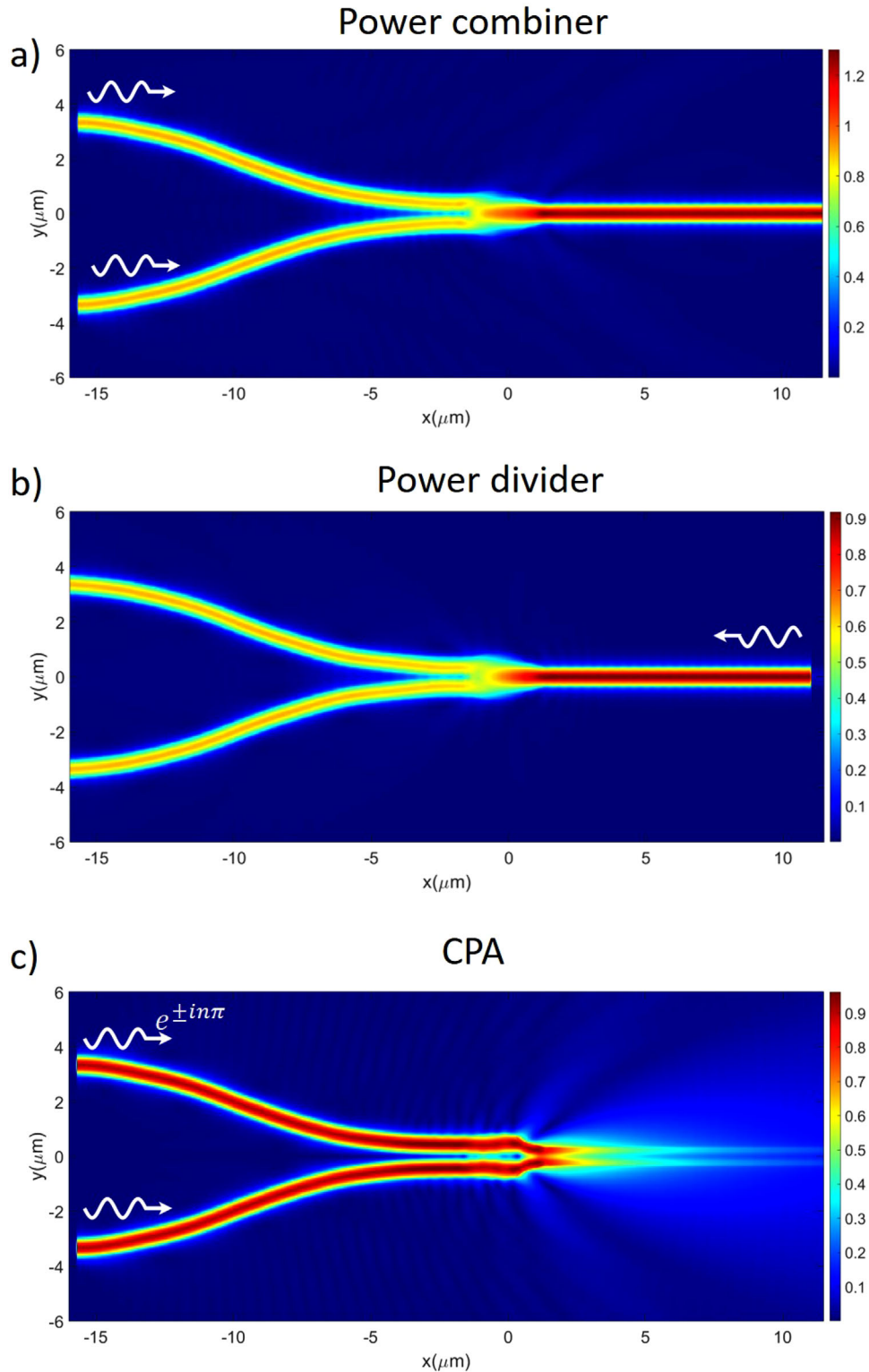
ADVANCED
SCIENCE NEWS

www.advancedsciencenews.com

LASER
& PHOTONICS
REVIEWS

www.lpr-journal.org

Power combiner

a)

Power divider

b)

CPA

c)

Figure 4. Absolute value of the E-field in the middle plane of the device at $\lambda = 1.55 \, \mu m$ for the designed WPD considering a) in-phase excitations through ports 2 and 3 (operation as a power combiner), b) excitation through port 1 (operation as a power divider), and c) out-of-phase excitation through ports 2 and 3 (operation as a CPA).
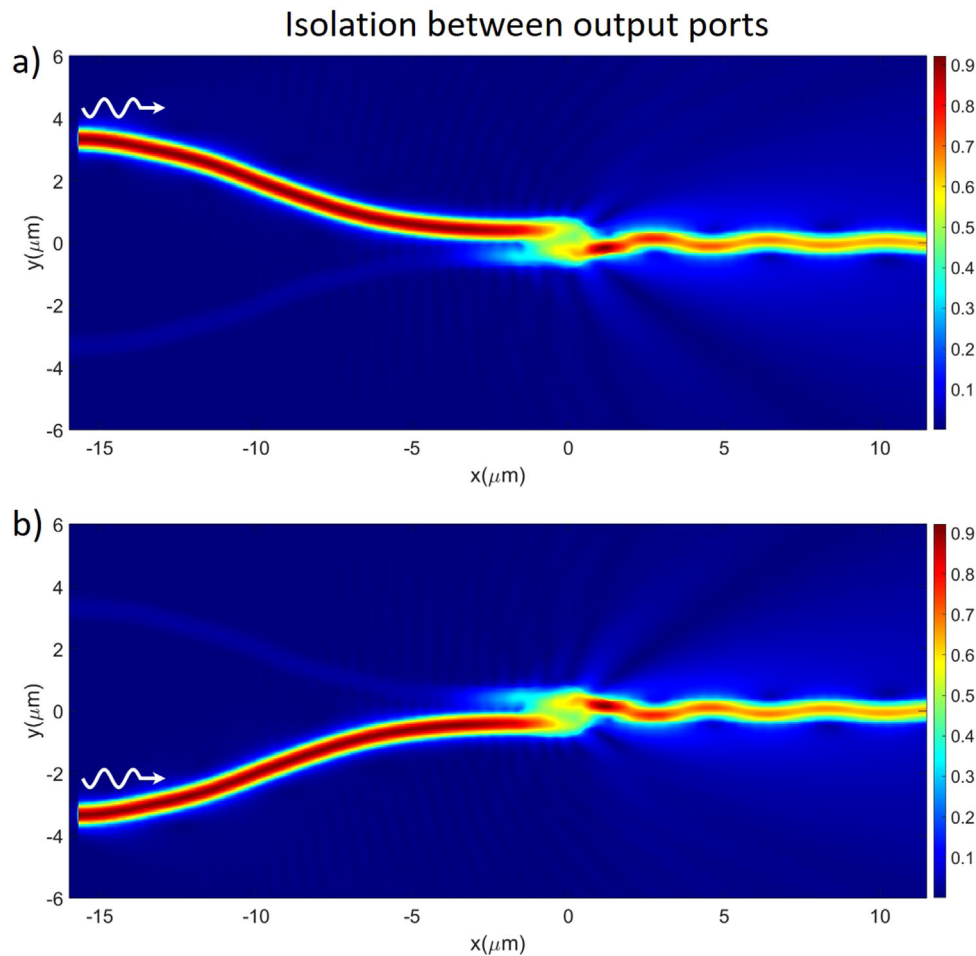
2200095 (7 of 10)

Isolation between output ports

Figure 5. Absolute value of the E-field in the middle plane of the device at $\lambda = 1.55 \, \mu m$ in the designed WPD for individual excitation of a) port 2 and b) port 3.

mented in a standard SOI platform, that is, a 220nm-thick silicon Y-branch, embedded in SiO_2 insulator. Each splitter branch consists of 600 nm wide × 220 nm high waveguides, connected by a 3-μm-length taper of 0.6 μm width at the input and 1.2 μm at the output. The taper geometry is constructed by specifying a set of taper widths $\{w_n\}$ along its length, and their subsequent interpolation to conform a smooth curve (see Figure 3b). **Table 1** summarizes the exact values of the design parameters.

Next, we discuss the performance of the device as predicted by FDTD numerical simulations.[51] Figure 3c depicts the absolute value and phase of the scattering matrix of the simulated WPD, at the operating wavelength of 1.55 μm. Comparison with the scattering matrix of the ideal WPD in Figure 3d confirms an excellent agreement between the designed and the ideal device. We note that there is an apparent deviation between their phases. However, such phase deviations correspond to scattering parameters with a near-zero absolute value, thus having no impact on the device operation.

The analysis of the electric field distribution in the simulated WPD provides additional physical insight and illustrates the operation principle of the WPD as predicted by the SVD of S in Equa-

tion (4). In particular, **Figure 4** depicts the operation of the device as i) a power combiner when excited in-phase through ports 2 and 3, ii) a power divider when excited through port 1, and iii) a coherent perfect absorber (CPA) for out-of-phase excitation through ports 2 and 3, leading to the radiation of all the power outside the device. Additionally, **Figure 5** confirms the existence of isolation between the output ports 2 and 3, by showing the field distributions when individually excited in ports 2 and 3. The asymmetric excitation of the WPD leads to i) the coupling of energy to a radiation mode and ii) successive field reflections along the output waveguide before stabilizing in the expected guided mode, as captured by the oscillations of the electric field in the output port 1.

In summary, we have shown that it is possible to take advantage of radiative losses to obtain the functionalities of a WPD within a pure silicon photonics platform. While the design of the device could be further optimized for a better performance, or to be adapted for a specific system, our results confirm that all CPA quantum state transformations can be implemented with a single device with reduced footprint and complexity, while being fully compatible with a SOI platform.

6. Conclusions

Our results have reported the quantum interference effects taking place in a Wilkinson power divider (WPD). To this end, we have revisited the classical mode of operation of a WPD by using an SVD decomposition of its scattering matrix, which highlights its classical operation as a power combiner, a power divider, and a CPA. The SVD also expedites the calculation of the quantum input–output relations and quantum interference processes in a WPD. We have demonstrated that a WPD grants access to CPA-based quantum state transformations. Specifically, we found that we can obtain single-photon CPA, two-photon nonlinear absorption, coherent absorption of N00N states, and quantum absorption of coherence in squeezed states. By contrast with previous implementations based on lossy beamsplitters, our results reveal that the same functionalities can be implemented on a compact device with a single output channel and no backward reflections. In turn, the use of a WPD reduces the complexity and number of elements of the CPA network. We have also shown through numerical FDTD simulations that we can implement a WPD on an SOI platform by taking advantage of radiative losses. We believe that our findings might help to experimentally demonstrate several CPA quantum interference effects that have only been theoretically reported. In general, we believe that our results are a good example on how optical components with advanced functionalities might contribute to the advancement of photonic quantum networks.

Conflict of Interest

The authors declare no conflict of interest.

Data Availability Statement

The data that support the findings of this study are available from the corresponding author upon reasonable request.

[1] J. Wang, F. Sciarrino, A. Laing, M. G. Thompson, *Nat. Photonics* **2020**, *14*, 273.

[2] J. Wang, S. Paesani, Y. Ding, R. Santagati, P. Skrzypczyk, A. Salavrakos, J. Tura, R. Augusiak, L. Mančinska, D. Bacco, D. Bonneau, J. W. Silverstone, Q. Gong, A. Acín, K. Rottwitt, L. K. Oxenløwe, J. L. O'Brien, A. Laing, M. G. Thompson, *Science* **2018**, *360*, 285.

[3] X. Qiang, X. Zhou, J. Wang, C. M. Wilkes, T. Loke, S. O'Gara, L. Kling, G. D. Marshall, R. Santagati, T. C. Ralph, J. B. Wang, J. L. O'Brien, M. G. Thompson, J. C. F. Matthews, *Nat. Photonics* **2018**, *12*, 534.

[4] H.-S. Zhong, H. Wang, Y.-H. Deng, M.-C. Chen, L.-C. Peng, Y.-H. Luo, J. Qin, D. Wu, X. Ding, Y. Hu, P. Hu, X.-Y. Yang, W.-J. Zhang, H. Li, Y. Li, X. Jiang, L. Gan, G. Yanglixing You, Z. Wang, L. Li, N.-L. Liu, C.-Y. Lu, J.-W. Pan, *Science* **2020**, *370*, 1460.

[5] C. Sparrow, E. Martín-López, N. Maraviglia, A. Neville, C. Harrold, J. Carolan, Y. N. Joglekar, T. Hashimoto, N. Matsuda, J. L. O.Brien, D. P. Tew, A. Laing, *Nature* **2018**, *557*, 660.

[6] Y. Chong, L. Ge, H. Cao, A. D. Stone, *Phys. Rev. Lett.* **2010**, *105*, 053901.

[7] D. G. Baranov, A. Krasnok, T. Shegai, A. Alù, Y. Chong, *Nat. Rev. Mater.* **2017**, *2*, 17064.

[8] X. Fang, M. Lun Tseng, J.-Y. Ou, K. F. MacDonald, D. Ping Tsai, N. I. Zheludev, *Appl. Phys. Lett.* **2014**, *104*, 141102.

[9] M. Papaioannou, E. Plum, J. Valente, E. T. Rogers, N. I. Zheludev, *APL Photonics* **2016**, *1*, 090801.

[10] S. Zanotto, F. Bianco, V. Miseikis, D. Convertino, C. Coletti, A. Tredicucci, *APL Photonics* **2017**, *2*, 016101.

[11] S. F. Liew, S. M. Popoff, S. W. Sheehan, A. Goetschy, C. A. Schmuttenmaer, A. D. Stone, H. Cao, *ACS Photonics* **2016**, *3*, 449.

[12] G. Pirruccio, M. Ramezani, S. R.-K. Rodriguez, J. G. Rivas, *Phys. Rev. Lett.* **2016**, *116*, 103002.

[13] A. N. Vetlugin, *Phys. Rev. A* **2021**, *104*, 013716.

[14] B. Vest, M.-C. Dheur, É. Devaux, A. Baron, E. Rousseau, J.-P. Hugonin, J.-J. Greffet, G. Messin, F. Marquier, *Science* **2017**, *356*, 1373.

[15] A. N. Vetlugin, R. Guo, C. Soci, N. I. Zheludev, *arXiv:2105.05444* **2021**.

[16] Q. Li, W. Bao, Z. Nie, Y. Xia, Y. Xue, Y. Wang, S. Yang, X. Zhang, *Nat. Photonics* **2021**, *15*, 267.

[17] T. Roger, S. Restuccia, A. Lyons, D. Giovannini, J. Romero, J. Jeffers, M. Padgett, D. Faccio, *Phys. Rev. Lett.* **2016**, *117*, 023601.

[18] B. Vest, I. Shlesinger, M.-C. Dheur, É. Devaux, J.-J. Greffet, G. Messin, F. Marquier, *New J. Phys.* **2018**, *20*, 053050.

[19] A. Lyons, D. Oren, T. Roger, V. Savinov, J. Valente, S. Vezzoli, N. I. Zheludev, M. Segev, D. Faccio, *Phys. Rev. A* **2019**, *99*, 011801.

[20] S. M. Barnett, J. Jeffers, A. Gatti, R. Loudon, *Phys. Rev. A* **1998**, *57*, 2134.

[21] A. Ü. Hardal, M. Wubs, *Optica* **2019**, *6*, 181.

[22] A. N. Vetlugin, R. Guo, A. Xomalis, S. Yanikgonul, G. Adamo, C. Soci, N. I. Zheludev, *Appl. Phys. Lett.* **2019**, *115*, 191101.

[23] T. Roger, S. Vezzoli, E. Bolduc, J. Valente, J. J. Heitz, J. Jeffers, C. Soci, J. Leach, C. Couteau, N. I. Zheludev, D. Faccio, *Nature Commun.* **2015**, *6*, 7031.

[24] W. Zhu, F. Xiao, M. Kang, M. Premaratne, *Appl. Phys. Lett.* **2016**, *108*, 121901.

[25] W. Zhu, I. D. Rukhlenko, F. Xiao, C. He, J. Geng, X. Liang, M. Premaratne, R. Jin, *Opt. Express* **2017**, *25*, 15737.

[26] M. J. Jung, C. Han, J. W. Yoon, S. H. Song, *Opt. Express* **2015**, *23*, 19837.

[27] A. Espinosa-Soria, E. Pinilla-Cienfuegos, F. J. Díaz-Fernández, A. Griol, J. Martí, A. Martínez, *ACS Photonics* **2018**, *5*, 2712.

[28] R. Bruck, O. L. Muskens, *Opt. Express* **2013**, *21*, 27652.

[29] S. Zanotto, A. Melloni, *J. Appl. Phys.* **2016**, *119*, 163103.

[30] W. Kang, Q. Gao, L. Dai, Y. Zhang, H. Zhang, Y. Zhang, *Results Phys.* **2020**, *19*, 103688.

[31] J. Zhang, C. Guo, K. Liu, Z. Zhu, W. Ye, X. Yuan, S. Qin, *Opt. Express* **2014**, *22*, 12524.

[32] Y. Fan, F. Zhang, Q. Zhao, Z. Wei, H. Li, *Opt. Lett.* **2014**, *39*, 6269.

[33] J. Luo, B. Liu, Z. H. Hang, Y. Lai, *Laser Photonics Rev.* **2018**, *12*, 1800001.

[34] W. Ji, D. Wang, S. Li, Y. Shang, W. Xiong, L. Zhang, J. Luo, *Appl. Phys. A* **2019**, *125*, 129.

[35] J. Jeffers, *J. Mod. Opt.* **2000**, *47*, 1819.

[36] D. M. Pozar, *Microwave Engineering*, Wiley, New York **2011**.

[37] J. E. Gentle, *Numerical Linear Algebra for Applications in Statistics*, Springer, Cham **2012**.

[38] G. H. Golub, C. F. Van Loan, *Matrix Computations*, Vol. *3*, Johns Hopkins University Press, Baltimore, MD **2013**.

[39] R. A. Horn, C. R. Johnson, *Matrix Analysis*, Cambridge University Press, Cambridge **2012**.

[40] T. Gruner, D.-G. Welsch, *Phys. Rev. A* **1996**, *54*, 1661.

[41] L. Knöll, S. Scheel, E. Schmidt, D.-G. Welsch, A. V. Chizhov, *Phys. Rev. A* **1999**, *59*, 4716.

[42] O. Hernández, I. Liberal, *arXiv:2108.12160* **2021**.

[43] V. Shchesnovich, *Phys. Rev. Lett.* **2016**, *116*, 123601.

[44] C. L. Degen, F. Reinhard, P. Cappellaro, *Rev. Mod. Phys.* **2017**, *89*, 035002.

[45] B. J. Lawrie, P. D. Lett, A. M. Marino, R. C. Pooser, *ACS Photonics* **2019**, *6*, 1307.

[46] R. Loudon, *The Quantum Theory of Light*, Oxford University Press, Oxford **2000**.

[47] C. T. Lee, *Phys. Rev. A* **1990**, *42*, 1608.

[48] Y. Zhang, S. Yang, A. E.-J. Lim, G.-Q. Lo, C. Galland, T. Baehr-Jones, M. Hochberg, *Opt. Express* **2013**, *21*, 1310.

[49] Z. Xiao, X. Luo, P. H. Lim, P. Prabhathan, S. T. Silalahi, T.-Y. Liow, J. Zhang, F. Luan, *Opt. Express* **2013**, *21*, 16331.

[50] S. Tao, Q. Fang, J. Song, M. Yu, G. Lo, D. Kwong, *Opt. Express* **2008**, *16*, 21456.

[51] Lumerical Inc., https://www.lumerical.com/products/fdtd/, (accessed: January 2022).